Gas pressure and coating distance for nanohydroxyapatite deposition on stainless steel 316L using flame spray technique

Angga SAPUTRA[1], Utami D. SYAFITRI[2], Toto SUDIRO[3], Gerald E. TIMUDA[3], and Yessie W. SARI[1,*]

[1] *Department of Physics, Faculty of Mathematics and Natural Sciences. IPB University, Bogor, 16680, Indonesia*
[2] *Department of Statistics, Faculty of Mathematics and Natural Sciences. IPB University, Bogor, 16680, Indonesia*
[3] *Research Center for Physics, Indonesian Institute of Sciences (LIPI), Build. 442 Kawasan PUSPIPTEK, South Tangerang 15314, Indonesia*

*Corresponding author e-mail: yessie.sari@apps.ipb.ac.id

Abstract

Metal implant coating engineering is needed to improve the surface biocompatibility properties of metals. For this, coating metal surfaces with bioactive and biocompatible biomaterials will be an option. Having high biocompatibility as well as similarity in chemical properties, nanohydroxyapatite may be a candidate as biomaterials for coating the metal implant. The key to the success of metal implant plating is the formation of pores which increase the bioactivity and biocompatibility properties of the implant. In this study, nanohydroxyapatite was used to be coated on stainless steel type 316L (SS316L). To ensure that the coating works properly on the surface, an appropriate measure of gas and distance is required. The purpose of this study was to determine the possible firing distance and gas pressure of the flame spray coating technique. The X-ray diffractometer (XRD), scanning electron microscope - energy dispersive X-ray spectroscopy (SEM-EDS), and optical microscopy (OM) characterizations were carried out to determine the phase, morphology, and presence of pores. After coated product, hydroxyapatite dehydroxylation occurred which led to the tetracalcium phosphate (TTCP) and β-tricalcium phosphate (β-TCP) phases. The thickness decreases with the addition of gas pressure and the farther the firing distance the layer thickness decreases. Nanohydroxyapatite coating on a bone implant substrate can increase the porosity of the layer.

1. Introduction

Metal implants have been commercially applied to replace the damaged bone due to their excellent mechanical strength. Stainless steel type 316L (SS316L) has been widely applied as bone and dental implants. SS316L has superior corrosion resistance, smoothness, biocompatibility, and cleanability after electropolishing treatment [1]. Additionally, this metal has the advantage of being cheaper when compared to other implant metals. However, the nature of SS316L which is bioinert from an osteogenesis perspective may be one of the major concerns in its application. Being bioinert, SS316L thus could not promote the bone healing and new bone formation. For that, we need a material engineering to alter the bioinertness of SS316L. One effort that can be done is to coat the metal surface of SS316L with bioactive and biocompatible biomaterials. Surface coating of metal implants with biomaterials can modify the structural composition and morphology of the metal surface so that it is bioactive and bio-compatible and can maintain its mechanical properties. The key to the success of metal implant plating is the formation of pores which increase the bioactivity and biocompatibility properties of the implant [2-5].

The selection of the right metal implant coating biomaterial needs to be considered. One of the biomaterials that can be used as a coating for metal implants is hydroxyapatite. Hydroxyapatite [$Ca_{10}(PO_4)_6(OH)_2$] (HAp) is a biocompatible and bioactive ceramic [6].

The choice of HAp was caused by calcium phosphate compounds which are analogous to inorganic compounds in human bones [7] hence it is appropriate to be used as a metal coating for SS316L. The development of nanotechnology has made a good contribution to biomaterial engineering. Nanohydroxyapatite has higher bioactivity and biocompatibility compared to micro-size hydroxyapatite [8,9]. Calcium sources and synthesis techniques to obtain nanohydroxyapatite powder have been widely used. The use of biowaste materials will certainly provide added value, such as increasing economic value, and reducing the environmental pollution. The microwave irradiation technique in the nanohydroxyapatite synthesis process is proven to be cost-effective, efficient, and the fastest technique in the whole process [10]. Therefore, in this study, domestic duck eggshells were used as a source of calcium and microwave irradiation techniques to obtain nanohydroxyapatite powder.

Thermal spray coating is the most important technique for surface modification. In general, the uniform layer thickness is influenced by many factors including the spraying process, the fuel mixture of acetylene and oxygen gas, etc. Commonly the use of thermal spray coating processes includes detonation gun spray, flame spray, high-velocity oxy-fuel spray, plasma spray, wire arc spray, and cold spray. All thermal spraying processes can be used according to the required properties, consider the price and suitability of the process for certain materials. Flame spraying is the oldest thermal spraying process,

Table 1. Summary of thermal spray methods and parameters in several studies.

Method	Coating distance (cm)	Coating thickness (µm)	Porosity (%)	Reference
Plasma spray	8.5 - 1.15	194 - 270	4 - 8	[20]
Atmospheric plasma (APS)	8 - 12	159 - 178	0.2 - 1.1	[21]
High velocity oxygen-fuel (HVOF)	20 - 25	279 - 429	1.3 - 3.7	[21]
High-velocity suspension flame spraying (HVSFS)	12.5	81 - 133	4.1 - 8.9	[21]
Thermal spraying equipment (CERAJET)	10	108 - 140	-	[13]
Plasma spray	7.5	150	-	[22]
Vacuum plasma spray	25	35 - 160	1.18 - 3.86	[23]

characterized by low capital investment, high efficiency and deposition rates, and relatively easy operation and low maintenance costs. The flame spray coating (FSC) technique is widely used for corrosion protection or coating on structures and machine parts, bridges, offshore platforms, and LPG cylinders. Among the various hydroxyapatite coating techniques, thermal spraying is the only technique approved by the Food and Drug Administration (FDA) for biomedical implant materials [11-13].

The coating thickness and porosity become the parameters that are very important in the surface coating technique of metal implants. Both of these are closely related to the infiltration, bioactivity, and osteoconductivity process. The thickness of $50 < x < 200$ µm has long-them stability [14] and porosity between 30-50% has been shown to promote excellent tissue growth [15 - 19]. Several studies of hydroxyapatite coating on metal implants using thermal spray methods are summarized in Table 1. The coating distance that has been used is 7.5-25 cm and the resulting thickness was 35-429 µm. However, the resulting porosity is still very low, in the range of 0.2-8.9%. Therefore, further research is needed to obtain high porosity. The FSC method has the advantage of obtaining porosity >10% [22].

In this study, nanohydroxyapatite was synthesized from duck eggshells as a calcium source. Nanohydroxyapatite was used to be coated on SS316L as a substrate. To ensure that the coating works properly on the surface, an appropriate measure of gas and distance is required. The purpose of this study is to determine the possible firing distance and gas pressure from the flame spray coating technique in order to obtain better thickness and porosity. The outcomes of this study is expected to serve as the basis for further optimization in metal implant coating with nanohydroxyapatite.

2. Experimental

2.1 Materials

The materials used for the nanohydroxyapatite synthesis were duck eggshells as a calcium source and phosphoric acid (H_3PO_4, Merck) as a phosphoric source. Stainless steel type 316L (SS316L) was used as the metal implant substrate.

2.2 Synthesis and characterization of nanohydroxyapatite

The initial stage of nanohydroxyapatite synthesis was the calcination of duck eggshells. It was carried out in the muffle furnace (Nabertherm B180) to change the $CaCO_3$ phase to CaO and also to remove the organic components of the sample. The calcined sample was then deposited by $Ca(OH)_2$ 1 M and H_3PO_4 0.6 M with a Ca to P ratio of 1.67. The mixture was immediately transferred into a microwave oven with power 400 W for 45 min. Afterward, the result was sintered at 900°C for 5 h and then ground using a mortar and filtered using a 100 mesh sieve. Nanoydroxyapatite powder was analyzed by an X-ray diffractometer (XRD) (RIGAKU, SMARTLAB) using CuKα (1.541862 Å) at 40 kV and 30 mA. The data were collected in the 2θ range of 10°-90° with scan step width 0.01° and speed 0.3 s. The surface morphology of nanohydroxyapatite was observed by using scanning electron microscope (SEM) (Hitachi, SU-3500) at an accelerating voltage of 20 kV. Energy dispersive X-ray spectroscopy (EDS) was used to analyze the nanohydroxyapatite elemental composition.

2.3 Deposition of nanohydroxyapatite coating on SS316L

SS316L was cut into 15 x 15 x 3 mm pieces. The surface of the SS316L was polished using sandpaper 320, 400, 800, 1000, and 1200 grit, sequentially. After that, the substrate was sandblasted to remove the oxide scales and to make the surface rougher so that it is easy to be coated. Nanohydroxyapatite coatings were deposited on the surface of SS316L by flame spray coating technique (Metallisation Flamespray, MK74). In this system, acetylene and oxygen were used as combustion gases and the compressed air was used as the carrier gas to feed the nanohydroxyapatite powder from the hooper to the spray torch [13]. The deposition of nanohydroxyapatite on SS316L was conducted at carrier gas flow (acetylene: 2.3 bar and oxygen: 1.15 bar), varied gas pressure and coating distances as shown in Table 2.

2.4 Characterization of coated nanohydroxyapatite on SS316L

The phase structure of deposited nanohydroxyapatite on the SS 316L was carried out by X-ray diffractometer (XRD) characterization. In addition, scanning electron microscope - energy dispersive X-ray spectroscopy (SEM-EDS) analysis was carried out to determine the surface morphology and the elemental composition of coated nanohydroxyapatite on SS316L. The optical microscopy (OM) (Digital Microscope VHX-6000) analysis was used to observe the cross sectional of the sample. This analysis was carried out to examine the thickness of the coating layer and the porosity of the deposited nanohydroxyapatite. In this case, Fiji ImageJ software was used to analyze the layer thickness and coating porosity.

Table 2. Deposition parameters of nanohydroxyapatite coatings on SS316L.

Sample code	Gas pressure (bar)	Coating distance (cm)
A-2-15	2	15
B-1-20	1	20
B-2-20	2	20
C-2-25	2	25
C-3-25	3	25
D-2-30	2	30
D-3-30	3	30

3. Results and discussion

3.1 XRD and SEM-EDS analysis of hydroxyapatite powder

Figure 1 presents XRD patterns of synthesized hydroxyapatite and has been compared with JCPDS (Joint Committee on Powder Diffraction) card no 09-432. The three peaks having highest intensity appears at $2\theta = 31.799°$, $32.212°$, and $32.929°$ corresponding to (211), (112), and (300) crystal planes, respectively. It can be seen that all diffraction peaks belong to hydroxyapatite reflection. These results suggest that high purity hydroxyapatite was successfully synthesized.
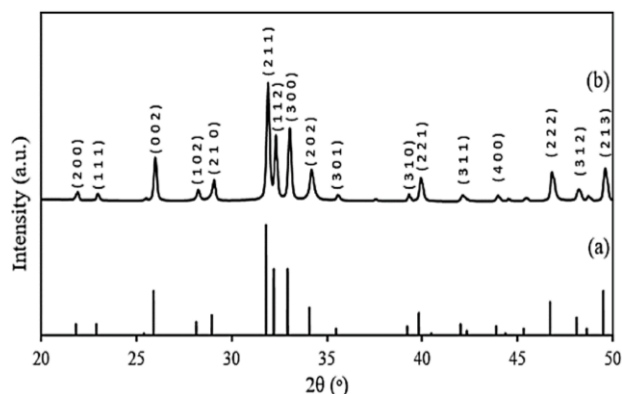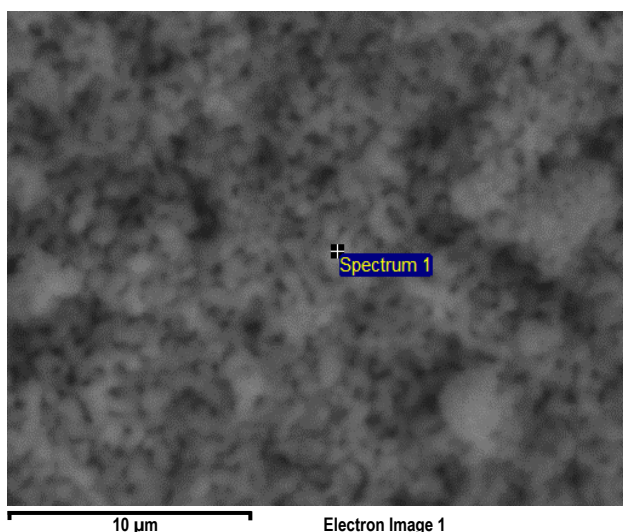

Figure 1. XRD patterns of hydroxyapatite: (a) JCPDS and (b) synthesis.

Figure 2. SEM image and corresponding energy dispersive EDS point analysis of nanohydroxyapatite powder (spectrum 1).

Figure 2 presents the results of SEM-EDS point analysis of hydroxyapatite powder (spectrum 1). The SEM morphology of hydroxyapatite (HAp) powder shows oval shaped. The hydroxyapatite particle size is calculated using the Fiji ImageJ software from 20 points of about 104.00 ± 16.63 nm. It can be said that the particles are on a nanometer scale. The EDS analysis in Table 3 shows that the sample contained elements (wt%) of oxygen (O): 49.64%, phosphorous (P): 17.05%, and calcium (Ca): 33.31%. The detected element identified nanohydroxyapatite as having high purity.

Table 3. EDS point analysis of hydroxyapatite powder.

Elemental composition	Weight %
O	49.64
P	17.05
Ca	33.31

3.2 XRD and SEM-EDS analysis of flame sprayed nano-hydroxyapatite coating on SS316L

The XRD patterns of flame sprayed nanohydrxyapatite coating on SS316L substrate are shown in Figure 3. The results of XRD analysis shows that the phase consisted of HAp: (JCPDS card no. 09-0432), β-tricalcium phosphate (β-TCP JCPDS card no. 09-0169), tetracalcium phosphate (TTCP JCPDS card no 09-0432), and SS316L: (JCPDS card no 33-0397). In samples A-2-15, B-1-20, and B-2-20 the confirmed phases are HAp, β-TCP, and TTCP. In the C-2-25 sample, the confirmed phase is dominated by calcium phosphate compounds (HAp, β-TCP, and TTCP), but there is a confirmed SS316L phase. This means that the hydroxyapatite is not coated completely. In samples C-3-25, D-2-30, and D-3-30 the confirmed phase are SS316L with high peak intensity and a little confirmed hydroxyapatite phase.

In the samples A-2-15, B-1-20, B-2-20, and C-2-25, the HAp is decomposed into β-TCP and TTCP. However, in the C-3-25, D-2-30, and D-3-30 samples, no β-TCP and TTCP phases are seen. Thus, the firing distance and gas pressure can affect the HAp decomposition process. Decomposition occurs at a firing distance of 15 cm, 20 cm, and 25 cm, so that it is associated with high deposition temperatures. This happens because the closer the coating distance, the higher the temperature of the substrate and the material being deposited. In addition, gas pressure also affects the decomposition of HAp into β-TCP and TTCP phases. In sample B-1-20 the TTCP phase is detected, but in sample B-2-20 it is not. In addition, the β-TCP phase is detected in sample C-2-25, but not in sample C-3-25. This means, the smaller the pressure, the possibility that the decomposition of HAp to β-TCP or TTCP will occur.
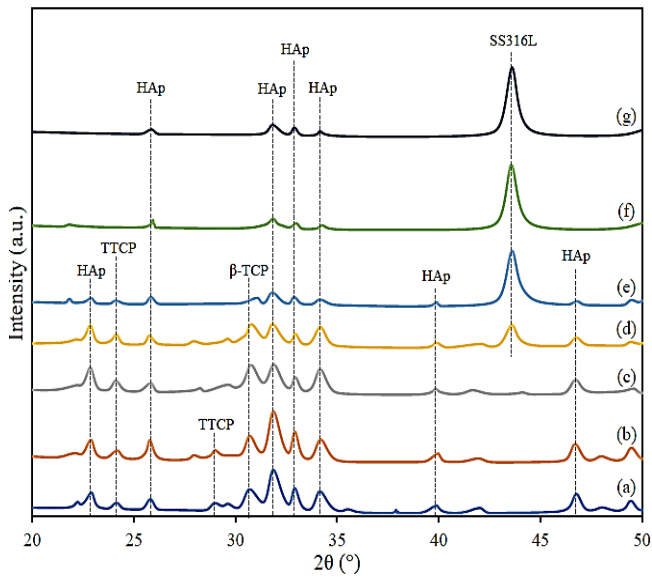
Figure 3. XRD patterns of flame sprayed nanohydroxyapatite coating on SS316L (a) A-2-15, (b) B-1-20, (c) B-2-20, (d) C-2-25, (e) C-3-25, (f) D-2-30, and (g) D-3-30.

The decomposition of HAp coatings is related to the high temperature during the thermal flame spraying. In thermal sprayed HAp coatings, process-related variability has shown a significant effect on coating characteristics such as phase composition, structure, and chemical composition. In subsonic thermal sprayed HAp coatings, it was shown that dehydroxylation of HAp leads to TTCP and β-TCP phases [13]. The change in the HAp phase to β-TCP or TTCP is certainly not expected. However, β-TCP and TTCP are still calcium phosphate compounds that have bioactive and biocompatible properties. β-TCP is less stable than HAp but has a faster degradation rate and higher solubility. In addition, it has a high resorption rate and is widely used to increase biocompatibility. The characteristics of β-TCP have been actively studied for bone regeneration purposes, and β-TCP has been widely used in bone cements and bone substitution [25]. TTCP scaffolds had good biocompatibility. TTCP scaffolds may be a promising candidate for bone regeneration applications [26]. Liu *et al.* 2019 [27] reported that TTCP into magnesium phosphate (MPC) enhanced the efficiency of new bone formation. TTCP/MPC also showed good biocompatibility, biodegradability, and osteoconductivity with host bone in vivo. Thus, the change in the hydroxyapatite phase to β-TCP and TTCP is not a significant problem in its application because it is still biocompatible.
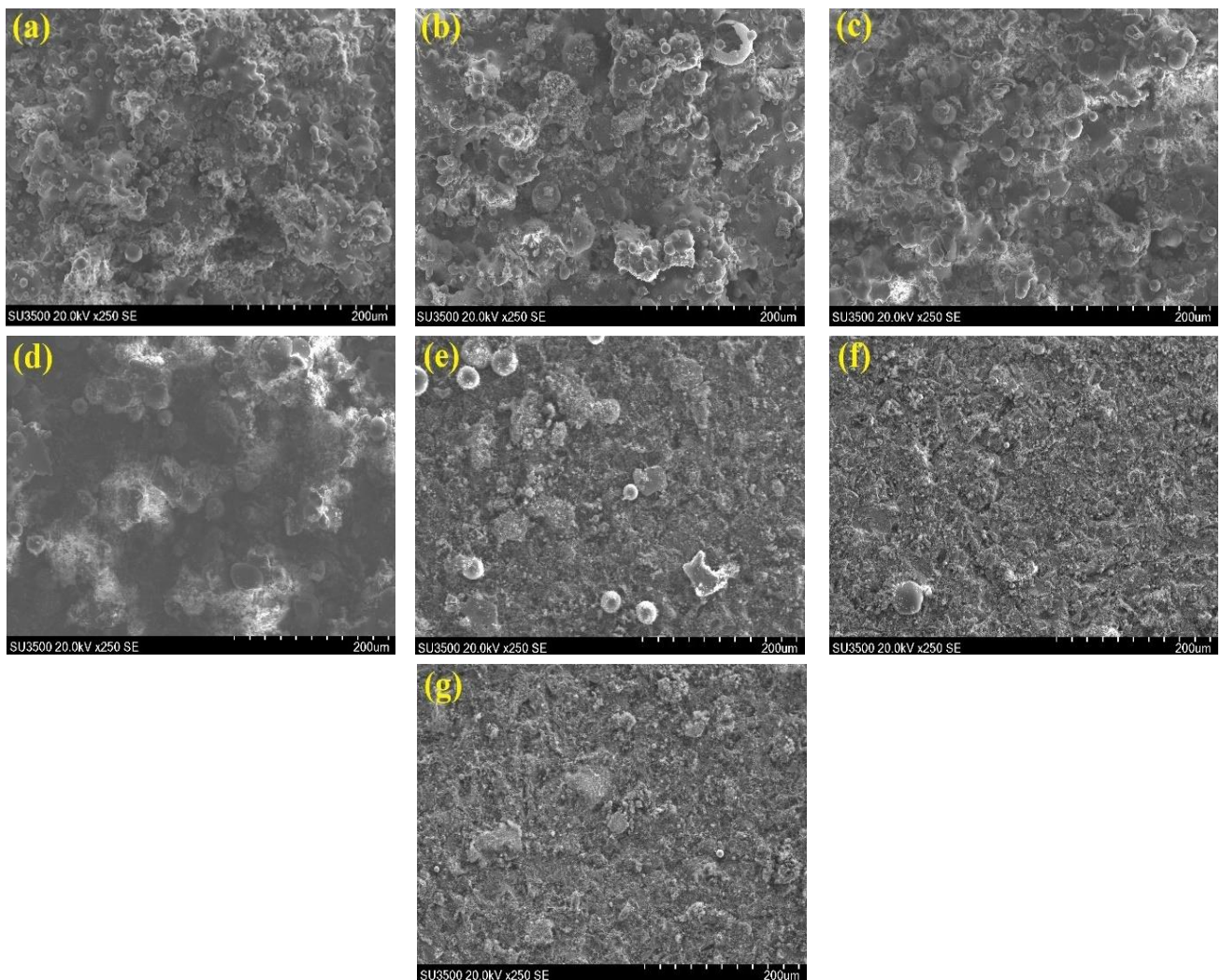

Figure 4. SEM morphologies of flame sprayed nanohydroxyapatite coating on SS316L (a) A-2-15, (b) B-1-20, (c) B-2-20, (d) C-2-25, (e) C-3-25, (f) D-2-30, and (g) D-3-30.

The SEM morphologies of flame sprayed nanohydroxyapatite coating on SS316L shown in Figure 4. The morphologies showed that mostly the nanohydroxyapatite are melted, and it mainly consists of fine spherical and semispherical particles on samples A-2-15, B-1-20, and B-2-20. The molten powder particle into very fine spherical particles due to the impact of a high-speed plasma jet and the impact of striking on the implant surface [28]. However, the presence of pores on the surface will increase bioactivity and osteoconductivity. In samples C-2-25 and C-3-25 there are a large sphere, however uncoated on all surfaces. However, on the D-2-30 and D-3-30 samples, there were no such particles at all. In Table 4, the sample A-2-15, B-1-20, and B-2-20 elemental composition observed are O, P, and Ca. This element is the same as that found in the energy dispersive X-ray spectroscopy (EDS) hydroxyapatite analysis results. Figure 5 and Figure 6 presents SEM images and corresponding EDS point analysis of flame sprayed nanohydroxyapatite coating on SS316L.

Therefore, all SS316L substrate surfaces are not completely coated. Figure 5 presents SEM images and corresponding EDS point analysis of flame sprayed nanohydroxyapatite coating on SS316L sample C-2-25. Table 5 shows the EDS analysis for spectrum 5 and spectrum 6. In spectrum 5, the detected elemental compositions are O, P, and Ca as well as the hydroxyapatite EDS results. However, in Spectrum 6, the detected elemental compositions are Cr, Mn, Fe, Ni, Si, C, etc. These elements are similar to the elements found in SS316L. Metallurgical condition composition (wt%) plate SS316L (ASTM, 2003) were bal. Fe, 16 - 18.5 Cr, 10 - 14 Ni, 2 - 3 Mo, < 2 Mn, < 1 Si, and < 0.03 C [29]. Thus, the results of the EDS analysis confirm that the C-2-25 HAp sample is not completely coated. The part of the substrate that is not coated will be exposed to heat during coating. Thus, the substrate is oxidized to form Fe_2O_3 [30]. In addition, there are cracks that are certainly not expected here as they will reduce the binding strength of the layers.

Table 4. EDS point analysis of flame sprayed nanohydroxyapatite coating on SS316L sample A-2-15, B-1-20, and B-2-20.

Sample code	A-2-15	B-1-20	B-2-20
	Weight %	Weight %	Weight %
Elemental composition	Spectrum 4	Spectrum 3	Spectrum 6
O	37.78	41.92	40.29
P	19.70	19.89	18.78
Ca	34.33	32.19	34.37

Table 5. EDS point analysis of flame sprayed nanohydroxyapatite coating on SS316L sample C-2-25: spectrum 5 and spectrum 6.

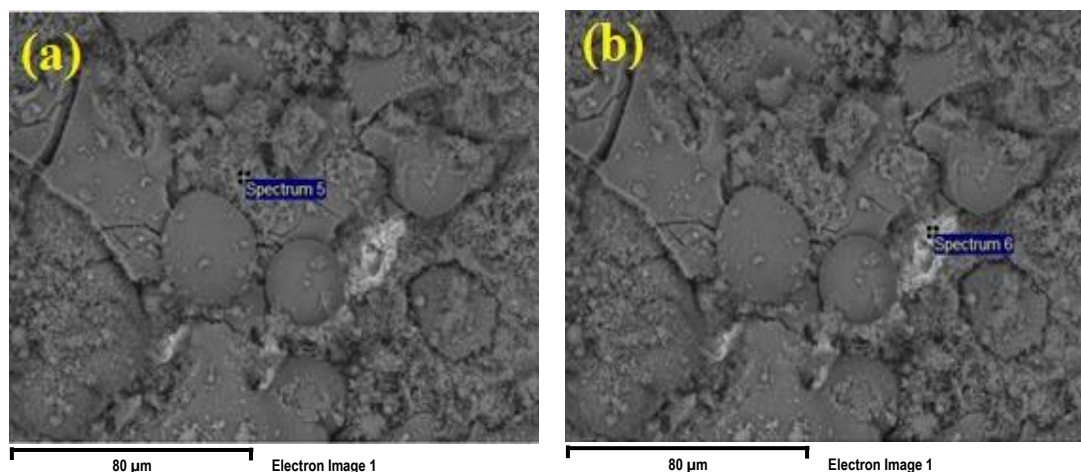| Elemental composition	Weight%	Weight%
	Spectrum 5	Spectrum 6
O	51.86	22.04
P	14.63	3.19
Ca	25.96	5.62
C	-	7.55
Mg	-	0.36
Al	-	1.13
Si	-	4.83
K	-	0.30
Cr	-	9.39
Mn	-	0.91
Fe	-	39.37
Ni	-	5.30

Figure 5. SEM images and EDS point analysis of flame sprayed nanohydroxyapatite coating on SS316L sample C-2-25 (a) spectrum 5 and (b) spectrum 6.
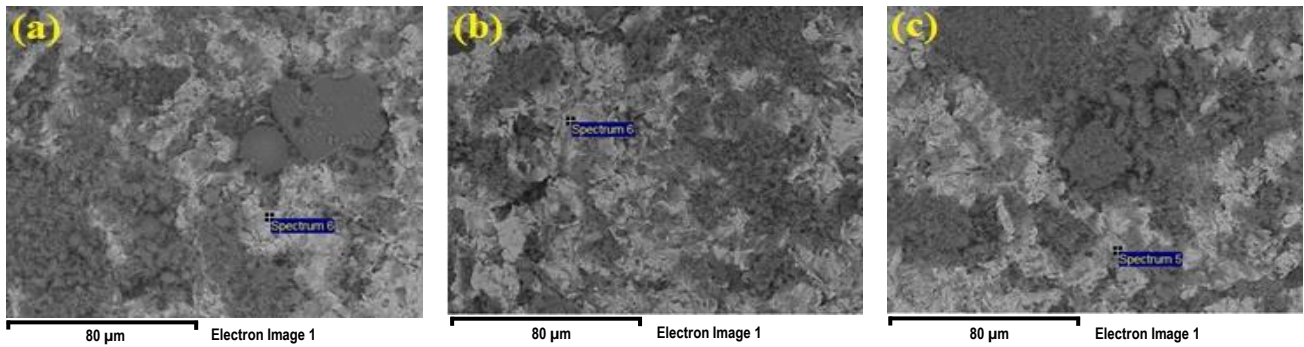
Figure 6. SEM images and corresponding EDS point analysis of flame sprayed nanohydroxyapatite coating on SS316L sample (a) C-3-25, (b) D-2-30, and (c) D-3-30.

Table 6. EDS point analysis of flame sprayed nanohydroxyapatite coating on SS316L sample C-3-25, D-2-30, and D-3-30.

Sample code	C-3-25	D-2-30	D-3-30
Elemental composition	Weight %	Weight %	Weight %
	Spectrum 6	Spectrum 6	Spectrum 5
C	5.29	8.88	9.58
O	14.56	8.28	6.19
Mg	0.27	0.38	-
Al	-	0.36	-
Si	0.54	0.63	0.30
P	3.74	0.71	0.76
Ca	5.2	1.38	1.43
Cr	13.17	14.67	14.61
Mn	1.31	1.45	1.43
Fe	49.69	55.04	56.09
Ni	6.23	7.83	7.80
Cu	-	0.39	-
Mo	-	-	1.81

It is different in Figure 6, in the samples C-3-25, D-2-30, and D-3-30, almost the entire surfaces are not coated with nanohydroxyapatite. Table 6 shows the energy dispersive X-ray spectroscopy (EDS) analysis for samples C-3-25, D-2-30, and D-3-30. All samples detected elemental compositions are similar to the elements found in SS316L. The white area in the SEM image is an area which indicates that the substrate is not coated with nanohydroxyapatite. Percentage of sample white area C-3-25: 43.41%, D-2-30: 45.04%, and D-3-30: 48.82%. The analysis results of the Fiji ImageJ software show that the farther the coating distance and the higher the gas pressure, the higher the white area or the area that is not coated with nanohydroxyapatite.

So, it can be said that samples with a firing distance of 15-20 cm and a gas pressure of 1-2 bar are better because the overall surface is coated with hydroxyapatite. The coating of the metal implant surface and the presence of pores will increase the bioactivity and osteo-conductivity of the metal implant surface. In addition, coated metal implants with hydroxyapatite will reduce the corrosion rate of metal implants.

3.2 OM analysis of cross-section nanohydroxyapatite coated on SS316L

Figure 7 presents cross-sectional OM images of flame sprayed nanohydroxyapatite coating on SS316L. The results of OM analysis showed that only samples A-2-15, B-1-20, and B-2-20 that are completely coated by nanohydroxyapatite. In the C-2-25 sample, the nanohydroxyapatite is not coated completely. Unlike the case with samples C-3-25, D-2-30, and D-3-30, nanohydroxyapatite are not coated completely on the substrate.

Table 7 presents the coating thickness and porosity of the nano-hydroxyapatite layer coated on SS316L. The coating thickness in Table 7 shows that gas pressure and firing distance greatly affect the thickness of the nanohydroxyapatite coated on the SS316L substrate. Coating thickness values are obtained using Fiji ImageJ software with 10 measurements, thickness values samples are A-2-15: 278.41 ±14.63 µm, B-1-20: 210.81 ±18.14 µm, B-2-20: 146.81 ±6.81 µm, and C-2-25: 31.65 ± 3.85 µm. The thickness decreases with the addition of gas pressure and the farther the firing distance the layer thickness decreases. The performance profile of plasma-sprayed nanohydroxyapatite coatings with thickness < 50 µm easy resorption and good adhesion. However, thickness 50-200 µm would be long-term stability, but reduced adhesion [14].

Fiji ImageJ software has been used to analyze porosity values. Processing of porosity analysis only on completely coated samples. The porosity samples are A-2-15: 28.23 ±2.50%, B-1-20: 35.54 ±3.45%, B-2-20: 41.44 ±0.76%. The porosity increases with the addition of gas pressure and the farther the firing distance the layer. The in vivo tested that material porosity fraction plays a crucial role in tissue ingrowth, highlighting that a 30% porosity provides an excellent tissue ingrowth proofed [15-17]. High macro-porosity

Table 7. Coating thickness and porosity of the nanohydroxyapatite layer coated on SS316L

Sample code	Coating thickness (µm)	Porosity (%)
A-2-15	278.41 ± 14.63	28.23 ± 2.50
B-1-20	210.81 ± 18.14	35.54 ± 3.45
B-2-20	146.81 ± 6.81	41.44 ± 0.76
C-2-25	31.65 ± 3.85	-
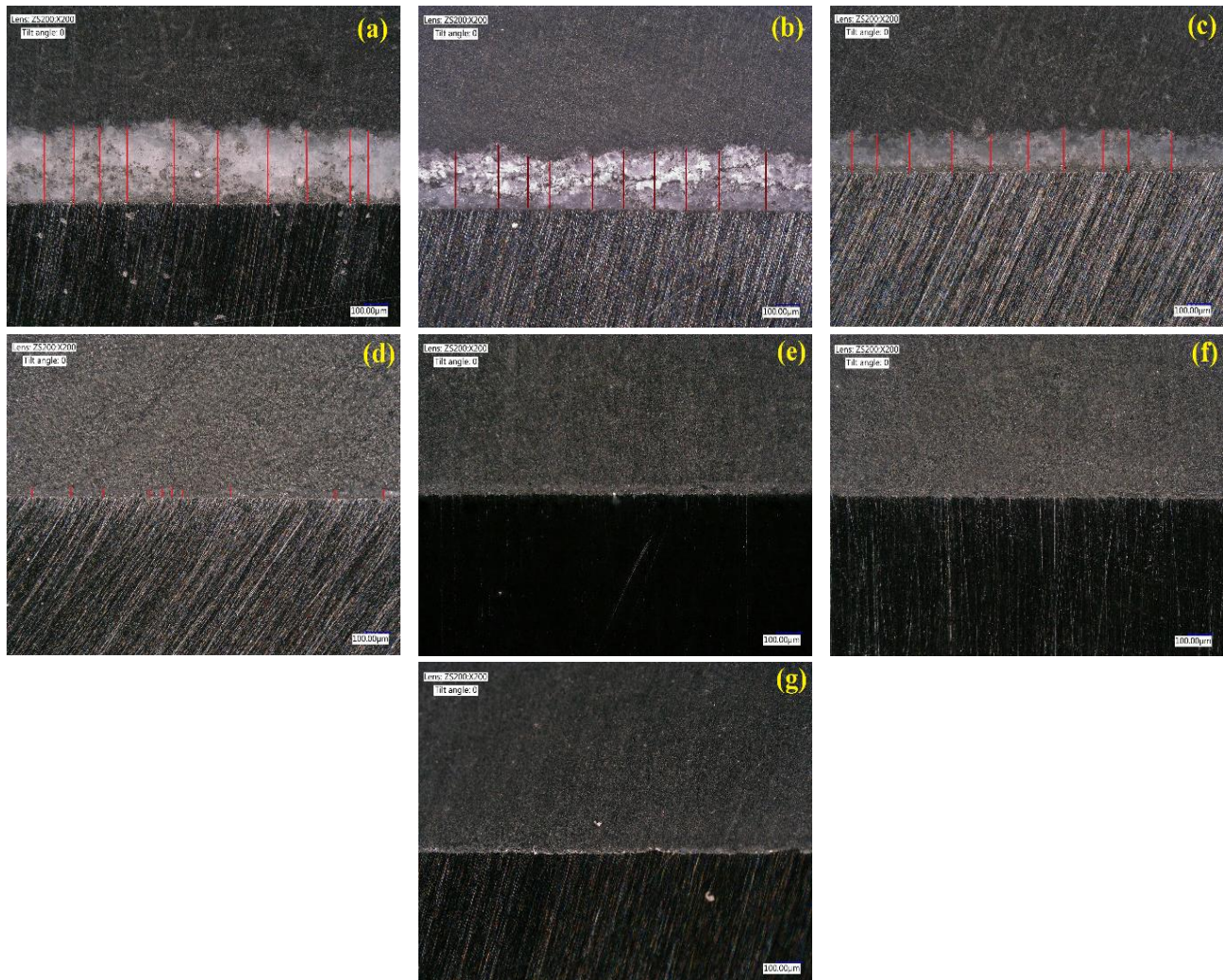
Figure 7. Cross-sectional OM images of flame sprayed nanohydroxyapatite coating on SS316L (a) A-2-15, (b) B-1-20, (c) B-2-20, (d) C-2-25, (e) C-3-25, (f) D-2-30, and (g) D-3-30.

can increase bone formation, but porosity that is higher than 50% can result in the decreasing of the mechanical properties of a biomaterial [18,19]. Nanohydroxyapatite coating on a bone implant substrate can increase the porosity of the layer which indicates a good level of osteoconductivity and bioactivity. Most of the resulting porosity is in the range 30-50%. Of course, this porosity value is very good for increasing bioactivity and osteoconductivity of metal implants and is much better than previous studies.

4. Conclusions

Deposition nanohydroxyapatite on the SS316L substrate had been successfully using a flame spray coating technique. The thickness decreases with the addition of gas pressure and the farther the firing distance the layer thickness decreases. However, it was different with porosity, the porosity increases with the addition of gas pressure and the farther the firing distance the layer. The possible firing distance and gas pressure of the deposition flame spray coating technique were at distance of 20 cm and varied gas pressure, 1-2 bar. Further information, nanohydroxyapatite coating on a bone implant substrate can increase the porosity of the layer.

Acknowledgements

References

[1] T. Hryniewicz, K. Rokosz, and M. Filippi, "Biomaterial studies on AISI 316L stainless steel after magnetoelectropolishing," *Materials*, vol. 2, pp. 129-145, 2009.

[2] N. Godbole, S. Yadav, M. Ramachandran, and S. Belemkar, "A review on surface treatment of stainless steel orthopedic implants," *International Journal of Pharmaceutical Sciences Review and Research*, vol. 36, pp. 190-194, 2016.

[3] V. Huynh, N. K. Ngo, and T. D. Golden, "Surface activation and pretreatments for biocompatible metals and alloys used in biomedical applications," *International Journal of Biomaterials*, vol. 3806504, pp. 1-21, 2019.

[4] N. S. Manam, W. S. W. Harun, D. N. A. Shri, S. A. C. Ghani, T. Kurniawan, M. H. Ismail, and M. H. I. Ibrahim, "Study of corrosion in biocompatible metals for implants: a review," *Journal of Alloys and Compounds*, vol. 701, pp. 698-715, 2017.

[5] E. Mohseni, E. Zalnezhad, and A. R. Bushroa, "Comparative investigation on the adhesion of hydroxyapatite coating on Ti–6Al–4V implant: Areview paper," *International Journal of Adhesion & Adhesives*, vol. 48, pp. 238-257, 2014.

[6] A. Parsapour, S. N. Khorasani, and M. H. Fathi, "Corrosion Behavior and Biocompatibility of Hydroxyapatite Coating on H_2SO_4 Passivated 316L SS for Human Body Implant," *Acta Metallurgica Sinica (English Letters)*, vol. 26, pp. 409-415, 2013.

[7] V. K. Mishra, S. K. Srivastava, B. P. Asthana, and D. Kumar, "Structural and spectroscopic studies of hydroxyapatite nanorods formed via microwave-assisted synthesis route," *Journal of the American Ceramic Society*, vol. 95, pp. 2709-2715, 2012.

[8] B. Ghiasi, Y. Sefidbakht, and M. Rezaei, "Hydroxyapatite for Biomedicine and Drug Delivery," *Advanced Structured Materials*, vol. 104, pp. 85-120, 2019.

[9] X. Gao, C. Dai, W. Liu, Y. Liu, Ru. Shen, X. Zheng, K. Duan, J. Weng, and S. Qu, "High-scale yield of nano hydroxyapatite through combination of mechanical activation and chemical dispersion," *Journal of Materials Science: Materials in Medicine*, vol. 28, pp. 1-9, 2017.

[10] N.A. Sajahan, and W.M.A.W. Ibrahim, "Microwave irradiation of nanohydroxyapatite from chicken eggshells and duck eggshells," *The Scientific World Journal*, vol. 275984 pp. 1-7, 2014.

[11] R. Kumar, and S. Kumar, "Thermal spray coating: a study," *International Journal of Engineering Sciences & Research Technology*, vol. 7, pp. 610-617, 2018.

[12] Y.C. Liu, G.S. Lin, J.Y. Wang, C.S. Cheng, Y.C. Yang, B.S. Lee, and K.L. Tung, "Synthesis and characterization of porous hydroxyapatite coatings deposited on titanium by flame spraying," *Surface and Coatings Technology*, vol. 349, pp. 357-363, 2018.

[13] T.P. Singh, H. Singh, and H. Singh, "Characterization of thermal sprayed hydroxyapatite coatings on some biomedical implant materials," *The Journal of Applied Biomaterials & Functional Materials*, vol. 12, pp. 48-56, 2014.

[14] R.B. Heimann, "Plasma-sprayed hydroxylapatite-based coatings: chemical, mechanical, microstructural, and biomedical properties," *Journal of Thermal Spray Technology*, vol. 25, pp. 827-850, 2016.

[15] A. Bandyopadhyay, F. Espana, V.K. Balla, S. Bose, Y. Ohgami, and N.M. Davies, "Influence of porosity on mechanical properties and in vivo response of Ti6Al4V implants," *Acta Biomaterialia*, vol. 6, pp. 1640-1648, 2010.

[16] A. Deing, B. Luthringer, D. Laipple, T. Ebel, and R. Willumeit, "A porous TiAl6V4 implant material for medical application," *International Journal of Biomaterials*, pp. 1-9, 2014.

[17] Y. Chena, J. Frith, A.D. Manshadia, H. Attara, and D. Kenta, "Mechanical properties and biocompatibility of porous titanium scaffolds for bone tissue engineering," *Journal of the Mechanical Behavior of Biomedical Materials*, vol. 75, pp. 169-174, 2017.

[18] A. Oryan, S. Alidadi, A. Moshiri, and N. Maffulli, "Bone regenerative medicine: classic options, novel strategies, and future directions," *Journal of Orthopaedic Surgery and Research*, vol. 9, pp. 18, 2014.

[19] S. Siswanto, D. Hikmawati, U. Kulsum, D.I. Rudyardjo, R. Apsari, and A. Aminatun, "Biocompatibility and osteoconductivity of scaffold porous composite collagen-hydroxyapatite based coral for bone regeneration," *Open Chemistry*, vol. 18, pp. 584-590, 2020.

[20] O. Graßmann, and R.B. Heimann, "Compositional and microstructural changes of engineered plasma-sprayed hydroxyapatite coatings on Ti6Al4V substrates during incubation in protein-free simulated body fluid," *Journal of Biomedical Materials Research*, vol. 53, pp. 685-93, 2000.

[21] R. Gadow, A. Killinger, and N. Stiegler, "Hydroxyapatite coatings for biomedical applications deposited by different thermal spray techniques," *Surface and Coatings Technology*, vol. 205, pp. 1157-1164, 2010.

[22] Y. Kayali, O. Aslan, M. Karabaş, and S. Talaş, "Corrosion behaviour of single and doubble layer hydroxyapatite coatings on 316L stainless steel by plasma spray," *Protection of Metals and Physical Chemistry of Surfaces*, vol. 52, pp. 1079-1085, 2016.

[23] A. Singh, G. Singh, and V. Chawla, "Characterization and mechanical behaviour of reinforced hydroxyapatite coatings deposited by vacuum plasma spray on SS-316L alloy", *Journal of the Mechanical Behavior of Biomedical Materials*, vol. 79, pp. 273-282, 2018.

[24] G.J. Odhiambo, W.G. Li, Y.T. Zhao, and C.L. Li, "Porosity and its significance in plasma sprayed coating: A Review," *Coatings*, vol. 9, pp. 1-19, 2019.

[25] J. Jeong, J.H. Kim, J.H. Shim, N.S. Hwang, and C.Y. Heo, "Bioactive calcium phosphate materials and applications in bone regeneration," *Biomaterials Research*, vol. 23, pp. 1-11, 2019.

[26] T. Qin, X. Li, H. Long, S. Bin, and Y. Xu, "Bioactive tetracalcium phosphate scaffolds fabricated by selective laser sintering for bone regeneration applications," *Materials*, vol. 13, pp. 1-12, 2020.

[27] J. Liu, J. Liao, Y. Li, Z. Yang, Q. Ying, Y. Xie, and A. Zhou, "Bioactive tetracalcium phosphate/magnesium phosphate composite bone cement for bone repair," *Journal of Biomaterials Applications*, vol. 34, pp. 239-249, 2019.

SAPUTRA, A., et al.

[28] J. Singh, S.S. Chatha, and H. Singh, "Characterization and corrosion behavior of functional gradient hydroxyapatite coating," *Journal of Thermal Spray Technology,* vol. 27, pp. 1371-1380, 2018.

[29] H. Hermawan, D. Ramdan, and J.R.P. Djuansjah, "Metals for Biomedical Applications," *Biomedical Engineering - From Theory to Applications*, ed Prof. Reza Fazel: InTech, ISBN: 978-953-307-637-9, 2011.

[30] L. Shao, G. Xie, G. Zhang, X. Liu, W. Lu, G. He, and J. Huang, "Combustion of metals in oxygen-enriched atmospheres," *Metals,* vol. 10, pp. 1-14, 2020.